THESIS FOR THE DEGREE OF LICENTIATE OF ENGINEEINRG

Copper in Chemical-Looping Combustion (CLC) and Chemical-Looping with Oxygen Uncoupling (CLOU)

Mehdi Arjmand

CHALMERS

Division of Environmental Inorganic Chemistry

Department of Chemical and Biological Engineering

Chalmers University of Technology

Göteborg, Sweden 2012

Copper in Chemical-Looping Combustion (CLC) and Chemical-Looping with Oxygen Uncoupling (CLOU)

MEHDI ARJMAND

Division of Environmental Inorganic Chemistry

Department of Chemical and Biological Engineering

Chalmers University of Technology

SE-412 96 Göteborg

Sweden

Phone: +46 (0)31-772 1000

arjmand@chalmers.se

Cover: SEM micrograph of copper(II) aluminate ($CuAl_2O_4$) oxygen carrier subject to several reduction and oxidation cycles.

ABSTRACT

The chemical-looping combustion (CLC) and chemical-looping with oxygen uncoupling (CLOU) processes are attractive solutions for efficient combustion with inherent separation of carbon dioxide. These processes use a metal oxide as an oxygen carrier to transfer oxygen from an air to a fuel reactor where the fuel, or gasification products of the fuel, reacts with the oxygen carrier.

The feasibility of Al_2O_3 and $MgAl_2O_4$-supported CuO oxygen carriers for CLC and CLOU processes are investigated in this work. The reactivity of these oxygen carriers was evaluated in a laboratory-scale fluidized-bed at 900 and 925°C under alternating reducing and oxidizing conditions. For Al_2O_3-supported oxygen carriers, CuO reacted with the support forming copper(II) aluminate ($CuAl_2O_4$), which is also a viable oxygen carrier, although it has no oxygen uncoupling properties. In the case of $MgAl_2O_4$ as support, the oxygen carrier exhibited stable oxygen release due to the presence of intact CuO.

In order to establish the phase relationships in the Cu–Al–O system, the standard enthalpy of formation, ΔH_f^0, of $CuAl_2O_4$ was reassessed using thermogravimetry and differential scanning calorimetry (TGA/DSC) due to discrepancy in thermodynamic databases. The reducing and oxidizing pathways in the Cu–Al–O system and the reversibility of the phases during the redox process were also investigated. Here, the phase transformations were examined as a function of duration of the reduction period and oxygen concentration during the re-oxidation period. It was found that the $CuAl_2O_4$ is reduced to copper(I) aluminate ($CuAlO_2$; delafossite), Cu_2O and elemental Cu. The $CuAlO_2$ phase is characterized by slow kinetics for re-oxidation into CuO and $CuAl_2O_4$.

The rate of oxygen release and the rate of oxidation of the $MgAl_2O_4$-supported CuO oxygen carrier were determined in the temperature range of 850–900°C. Devolatilized wood char was used to facilitate oxygen release from the oxygen carrier in N_2-fluidization by maintaining low oxygen concentration around the particles. The Avrami-Erofeev mechanism was used to model the rates of oxygen release. However, during oxidation it was observed that the rate is limited by the oxygen supply, indicating rapid conversion of the oxygen carrier. From the obtained reaction rates, the total amount of the investigated oxygen carrier needed in the air and the fuel reactor is estimated to be between 73–147 kg MW_{th}^{-1}.

ACKNOWLEDGMENT

Mehdi Arjmand
Göteborg, November 2012

LIST OF PUBLICATIONS

This thesis is based on the following publications:

I. **Arjmand M**, Azad A-M, Leion H, Lyngfelt A, Mattisson T, "Prospects of Al_2O_3 and $MgAl_2O_4$-Supported CuO Oxygen Carriers in Chemical-Looping Combustion (CLC) and Chemical-Looping with Oxygen Uncoupling (CLOU)", *Energy & Fuels, 2011, 25 (11), 5493–5502*

II. **Arjmand M**, Azad A-M, Leion H, Mattisson T, Lyngfelt A, "Evaluation of $CuAl_2O_4$ as an Oxygen Carrier in Chemical-Looping Combustion (CLC)", *Industrial & Engineering Chemistry Research, 2012, 51 (43), 13924–13934*

III. **Arjmand M**, Knee C, Leion H, Mattisson T, "Standard Enthalpy of Formation of $CuAl_2O_4$ Revisited", *2012 – Submitted for publication*

IV. **Arjmand M**, Keller M, Leion H, Mattisson T, Lyngfelt A, "Oxygen Release and Oxidation Rates of $MgAl_2O_4$-Supported CuO for Chemical-Looping with Oxygen Uncoupling (CLOU)", *Energy & Fuels, 2012 – In press*

Mehdi Arjmand is the principal author of all papers, and performed all of the experimental work, data evaluation and majority of the writing. Anders Lyngfelt is the principal academic supervisor. Henrik Leion and Tobias Mattisson are the co-supervisors. The examiner is Jan-Erik Svensson from the division of Environmental Inorganic Chemistry, Chalmers University of Technology.

Other related publications and contributions <u>not</u> included in the thesis:

- **Arjmand M**, Leion H, Lyngfelt A, Mattisson T "Use of Manganese Ore in Chemical-Looping Combustion (CLC) – Effect on Steam Gasification", *International Journal of Greenhouse Gas Control, 2012, 8, 56-60*

- Ryden M, **Arjmand M**, "Continuous Hydrogen Production via Steam-Iron Chemical-Looping Process in a Circulating Fluidized-bed Reactor", *International Journal of Hydrogen Energy, 2012, 37 (6), 4843–4854*

- **Arjmand M**, Leion H, Mattisson T, Lyngfelt A, "ZrO$_2$-Supported CuO-based Oxygen Carriers for Chemical-Looping with Oxygen Uncoupling (CLOU), *Energy Procedia, 2013 - In press*[†]

- **Arjmand M**, Leion H, Mattisson T, Lyngfelt A, "Investigation of Different Manganese Ores in Chemical-Looping Combustion (CLC) for Solid Fuels", *Submitted for publication*[‡]

[†]*This paper was also presented as a poster at the 11th International Conference on Greenhouse Gas Control in Kyoto, Japan, 18-22 November 2012.*

[‡]*This paper was also presented orally at the 2nd International Conference on Chemical-looping in Darmstadt, Germany, 26-28 September 2012.*

CONTENTS

1   INTRODUCTION

1.1   The Greenhouse Effect and Global Warming

The increase in concentration of some greenhouse gases in the atmosphere is expected to cause global warming and thus create changes in the world's climate. As shown in Figure 1.1, the short wave radiation from the sun penetrates the atmosphere and reaches the earth's surface. As the earth's surface is heated up, long wave radiation is emitted which is subsequently absorbed by greenhouse gases such as water vapour, carbon dioxide, methane, nitrous oxide, and aerosols, thus trapping heat. At general thermal equilibrium conditions, this keeps the earth's surface warm at an average temperature of $17^\circ C$.

Figure 1.1 Entrapment of part of the heat radiated from the earth's surface by greenhouse gases.[1]

However, excessive emission of the above-mentioned gases could trap more heat, thus increasing the average temperature.

Correlations have been found between the global average temperature and CO_2 concentrations in the atmosphere. With increased use of fossil fuels for energy production,[3] measures need to be taken to reduce anthropogenic CO_2 emissions in order to decrease possible contribution to global warming. A major source for release of CO_2 in the atmosphere is the combustion of fossil fuels. Therefore, the intergovernmental panel on climate control (IPCC), has suggested a 50–85% reduction in total CO_2 emission by 2050 to limit the anticipated global temperature rise to $2^\circ C$.[4] A number of alternative technologies have been proposed to mitigate the rising levels of carbon dioxide in the atmosphere. Among these, carbon capture and storage (CCS) is considered one alternative, which in combination with increased use of renewable energy and increased energy efficiency, could help reduce emissions of greenhouse gases to the atmosphere.

1.2   Carbon Capture and Storage (CCS)

By definition, CCS is the capture, transportation and storage of CO_2 in underground storage

locations (Figure 1.2).[5] Pre-combustion, post-combustion and oxy-fuel combustion are among the most investigated technologies for the capture of CO_2 from power plants and other CO_2-intensive industries. Post-combustion involves the separation of CO_2 from the flue gas by e.g. chemical absorption using amines. In pre-combustion, the CO in the synthetic gas produced from gasification is transformed to H_2 and CO_2 via the water-gas shift reaction, giving a gas with mainly H_2 and CO_2. CO_2 is then separated from the H_2 prior to combustion. Oxy-fuel combustion

Figure 1.2 Carbon dioxide capture and transportation to underground for long-term storage.[2]

involves the removal of N_2 from the air stream and carrying out the combustion process in O_2 and recycled flue gas.[6]

The CO_2 capture technologies are in various stages of development and some of them are at a semi-commercial demonstration stage for CCS application.[6] However, these technologies have high costs and energy penalties caused by the gas separation, which as a result decreases the process energy efficiency and thus increases the electricity or final energy cost.[7] It is therefore favoured to investigate and develop other inexpensive CO_2-capture technologies.

1.3 Chemical-Looping Combustion (CLC) and Chemical-Looping with Oxygen Uncoupling (CLOU)

In contrast to the other solutions for the capture of CO_2, the chemical-looping combustion (CLC) process can give an essentially pure CO_2 stream from hydrocarbon combustion without any direct gas separation. In a CLC system, two reactors, a fuel reactor and an air reactor, are interconnected with an oxygen carrier circulating between these reactors.[8-10] When fuel and air are introduced into the reactors, the following overall reactions occur, i.e. reaction (1.1) in the fuel reactor, and reaction (1.2) in the air reactor,

$$(2n + m)Me_xO_y + C_nH_{2m} \rightarrow (2n + m)Me_xO_{y-1} + nCO_2 + mH_2O \tag{1.1}$$

$$2Me_xO_{y-1} + O_2 \rightarrow 2Me_xO_y \tag{1.2}$$
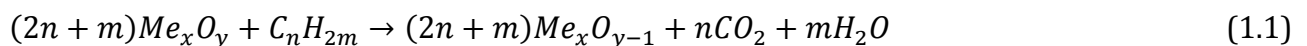
Here Me_xO_y and Me_xO_{y-1} are the oxidized and reduced forms of an oxygen carrier. The

scheme of the process is shown in Figure 1.3. In case of complete conversion of the fuel, the exhaust stream from the fuel reactor consists of only CO_2 and H_2O, from which pure CO_2 could be obtained after condensation of water. The reduced form of the oxygen carrier, Me_xO_{y-1}, is then transferred to the air reactor where it is re-oxidized by air making it ready for the next cycle. Thus in CLC, N_2 and CO_2 gases are never mixed.

The oxidation reaction is always exothermic while the reduction reaction can be exothermic or endothermic depending on the fuel and the oxygen carrier.[11] However, the sum of the heat from reactions (1.1) and
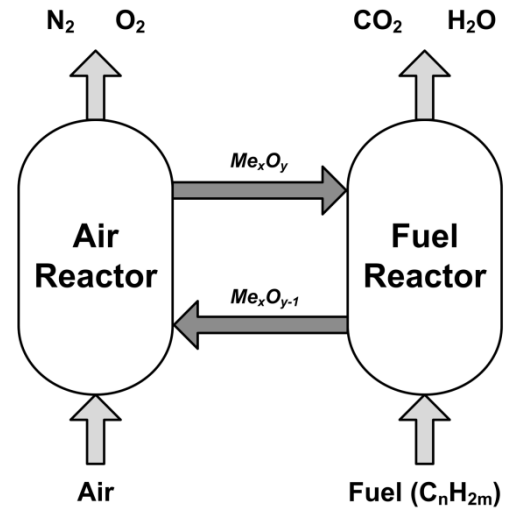
Figure 1.3 Schematic of the Chemical-Looping Combustion (CLC) process.

(1.2) is the same as for conventional combustion. Thus the CLC process does not entail any direct energy penalty for CO_2 separation. CLC has been successfully demonstrated in a number of units of sizes up to 120 kW.[12] Overviews of current achievements in CLC are given by Lyngfelt,[12, 13] Hossain and de Lasa[14] and Adanez et al.[15]

The CLC process can be used with gaseous, liquid or solid fuels. In the case of solid fuels, the char remaining after devolatilization is gasified in the presence of steam, producing CO and H_2 which can then react with the oxygen carrier. An alternative to CLC for solid fuels using gasification of the char, is chemical-looping with oxygen uncoupling (CLOU),[16] in which the char reacts directly with gaseous oxygen released from the oxygen carrier. In comparison to CLC where the reduction of oxygen carrier and oxidation of the gaseous fuel generally occurs in a single step, an additional step is needed in CLOU for the release of gaseous oxygen from the carrier prior to conversion of the fuel according to

$$Me_xO_y \rightarrow Me_xO_{y-2} + O_2 \tag{1.3}$$

This is followed by the normal combustion of the fuel via

$$C_nH_{2m} + \left(n + \frac{m}{2}\right)O_2 \rightarrow nCO_2 + mH_2O \tag{1.4}$$

The reduced oxygen carrier is transferred to the air reactor for re-oxidation. The net heat of reaction for the CLOU processes is the same as CLC and only the mechanism by which oxygen is accessed by the fuel differs. However when using solid fuels like coal, the CLOU process

avoids the slow gasification of the solid fuel needed to produce syngas as a prerequisite for the reaction with the oxygen carrier.[16] The oxygen carrier in CLOU must be able to release O_2 in the fuel reactor, but also be able to be oxidized in the air reactor at temperatures and oxygen concentrations suitable for the process, i.e. 800–1200°C. Conventional circulating fluidized bed (CFB) boilers often operate at an air ratio of 1.2,[8] which means that the oxygen concentration at the outlet of the air reactor in an equivalent CLC unit will be close to 5%. Therefore, oxide systems with an equilibrium partial pressure low enough for oxidation, i.e. below 5% O_2, are required. The oxide should also be able to release a significant concentration of oxygen in the fuel reactor. Therefore, such thermodynamic and kinetic requirements, limits the choice of oxygen carriers for the CLOU process.

A cornerstone in the development of CLC and CLOU processes is the oxygen carrier material. Thus, it is important to obtain a portfolio of inexpensive, durable oxygen carriers with sufficient reactivity. Oxides of transition metals (Mn, Fe, Co, Ni and Cu), their mixtures, and a number of natural minerals (ores), industrial wastes and by-products have been used as oxygen carriers in CLC and CLOU.[12-15] The reactivity of the oxygen carrier during oxidation and reduction and the ability to fully convert the fuel has been among the most sought-after criteria. In addition, thermal stability, mechanical strength, fluidizability and resistance to attrition and agglomeration are important. One way of achieving this for manufactured oxygen carriers is to mix the active phase (i.e. the reactive metal oxide) with an inert support such as TiO_2, SiO_2, ZrO_2, Al_2O_3 or $MgAl_2O_4$ and/or heat-treat the oxygen carriers.[14] Synthesized oxygen carriers also allow for a better control over the physical and chemical properties of the oxygen carrier during the manufacturing. However, the manufacturing cost for synthesized oxygen carriers may be of concern. When utilizing solid fuels in CLC, the lifetime of oxygen carrier particles is presumably affected by deactivation caused by ash or loss of material with the ash during separation from the oxygen carrier. Thus for CLC with solid fuels, less expensive natural minerals, industrial wastes and by-products with sufficient reactivity are favoured compared to more costly manufactured oxygen carriers.

1.4   Copper Oxide in CLC and CLOU

Copper oxide has received a great deal of attention as an efficient oxygen carrier, owing to its high reactivity during reduction and oxidation, high oxygen transport capacity and absence of thermodynamic limitation for complete combustion of the fuel. Considerable research has

been conducted using copper oxide as oxygen carrier in fluidized-bed[17-23] and fixed-bed[24, 25] batch reactors, continuous operation[26-30] and thermogravimetric studies,[19, 20, 31-36] with and without supports. Among various supports for CuO oxygen carriers, Al_2O_3 has received considerable attention.[18, 21, 22, 26, 28, 29, 32, 35-38] Many of the studies above have been conducted at conditions where there is no or very little release of oxygen via CLOU, for instance at low temperatures, and thus the focus has been on the direct gas-solid reaction between CuO and fuel.

In addition, $CuO–Cu_2O$ is one of the prominent oxide pairs suitable for the CLOU process.[16, 39] CuO decomposes to Cu_2O as per reaction (1.5) when the actual concentration of oxygen is lower than the equilibrium concentration (Table 1.1).[40]

$$4CuO \leftrightarrow 2Cu_2O + O_2 \qquad (1.5)$$

As a result, oxygen is released thereby making CLOU possible. It can be seen in Table 1.1 that the equilibrium O_2 concentration is a strong function of temperature.

Table 1.1 Equilibrium partial pressure of O_2 as a function of temperature for copper oxide.[41]

Temperature [^{o}C]	$P_{O_2,eq}$ [%]
850	0.5
875	0.9
900	1.6
925	2.7
950	4.6
975	7.6
1000	12.3

Some studies have also investigated the use of CuO oxygen carriers in CLC and CLOU for solid fuels.[16, 19, 20, 27, 37-39, 41-44]

Despite the attractive features of CuO as an oxygen carrier, its use is not without limitations. For example, copper oxide suffers from tendency towards agglomeration upon full reduction,[21] due to formation of elemental copper which has a rather low melting temperature (1085°C). In the case of Al_2O_3 as support, another difficulty arises due to the facile interaction between CuO and Al_2O_3 either during synthesis or during operation, resulting in partial loss of CuO by formation of copper(II) aluminate ($CuAl_2O_4$) and copper(I) aluminate ($CuAlO_2$; delafossite).[26, 28] Nevertheless, since the copper-aluminate phases are highly reducible,[22, 26, 28, 34, 45] the interaction between the support and the active phase does not cause any problem with respect to CLC application. For CLOU, however, this interaction needs to be avoided in order to preserve CuO as active phase. Since the interaction of CuO with Al_2O_3 seems to be difficult to avoid, other supports such as TiO_2, ZrO_2, SiO_2 or $MgAl_2O_4$ likely need to be employed for CLOU.[19, 20, 26-28, 33, 34, 39] Nonetheless, the use of Al_2O_3 as support for CuO oxygen carriers in CLC is favoured due to its abundance and lower cost (e.g. compared

to ZrO_2).

The knowledge of the reduction and oxidation rates is also of great importance in the design phase and for determination of the solids inventory in CLC and CLOU. It is important for the oxygen carrier to transport sufficient amount of oxygen from the air reactor to the fuel reactor in order to achieve complete conversion of the fuel. For the case of endothermic reactions in the fuel reactor, it is also essential to transport adequate heat to avoid excessive temperature drop. For CuO however, heat transport is not limiting since the overall reaction with fuel is exothermic.

1.5   *Aim of Study*

The main objective of this thesis is to provide a deeper understanding of the use of copper in CLC and CLOU. This thesis is based on the studies presented in papers I–IV. In paper I, a reactivity and feasibility study of four CuO-based oxygen carries using two different supports ($MgAl_2O_4$ and Al_2O_3) is carried out. The implication of the interaction of CuO with Al_2O_3 in CLC and CLOU is also briefly addressed in paper I. Paper II provides a more detailed investigation of the reaction pathways in the Cu–Al–O phase system for the CLC process using one of the oxygen carriers ($CuAl_2O_4$) from paper I. This required the relevant thermodynamic data to be reassessed, which is performed in the study presented in paper III. In paper IV, the rate of release of oxygen and oxidation, and the amount of solids needed is determined for the CLOU process using one of the oxygen carriers ($CuO/MgAl_2O_4$) from paper I.

2   EXPERIMENTAL DETAILS

2.1   *Preparation, Manufacturing and Characterization of the Oxygen Carriers*

The physical properties and characteristics of the oxygen carriers used in papers I–IV are summarized in Table 2.1. The particles were manufactured by freeze-granulation. Here a water-based slurry of CuO and support powders consisting of α-Al_2O_3 (A16SG, Alcoa) and $MgAl_2O_4$ (S30CR, Baikowski) with a weight ratio of 40/60 wt. % along with small amount of dispersant (Dolapix PC21) is prepared. After addition of binder, the subsequent mixture is ball milled for 24 h, prior to granulation. The slurry is then pumped through a spray nozzle and into liquid nitrogen to form spherical particles upon instantaneous freezing. The samples were calcined at 950 and 1050°C for 6 h at a ramp rate of 5°C min^{-1} and then sieved through stainless steel screens to obtain particles in the size range of 125–180 μm. The calcination temperatures are given in the abbreviation for each sample in Table 2.1.

The oxygen carriers were analyzed before and after the experiments using powder X-ray diffraction (XRD; Bruker AXS, D8 Advanced), environmental scanning electron microscope (ESEM; FEI, Quanta 200), N_2–absorption (Micromeritics, TriStar 3000) for determination of BET specific surface area, Hg–intrusion (Micromeritics, AutoPore IV 9500) for determination of porosity, force gauge (Shimpo, FGN-5X) for determination of crushing strength and light microscope (Nikon, SMZ800) for determination of particle size distribution (PSD) using ImageJ software.[46] The effective density of the particles, sized 125–180 μm, was measured assuming a theoretical void fraction of 0.37 of a packed-bed with uniform spherical particles. The crushing strength of all particles is found to be less than 0.5 N. However, this did not cause any problem with respect to fragmentation of particles during the experiments.

Table 2.1 Physical properties and characteristics of the oxygen carriers used in papers I–IV.

Oxygen Carrier	C4A-950	C4A-1050	C4MA-950	C4MA-1050
Effective density [g cm^{-3}]	2.4	1.3	2.1	2.6
BET specific surface area [m^2 g^{-1}]	4.1	4.2	11.7	6.5
Porosity [%]	–	–	47.6	–
Crystalline phase identified by XRD	CuO, α-Al_2O_3, $CuAl_2O_4$*	$CuAl_2O_4$, α-Al_2O_3, CuO*	CuO, $MgAl_2O_4$	

* minor phase

2.2   *Experimental Setup and Procedure*

The experiments in papers I, II and IV were carried out in a quartz fluidized-bed reactor, 870 mm long and 22 mm in inner diameter. A porous quartz plate was placed at a height of 370 mm from the bottom and the reactor temperature was measured with chromel-alumel (type K) thermocouples sheathed in inconel-600 located about 5 mm below and 25 mm above the plate. Honeywell pressure transducers with a frequency of 20 Hz were used to measure

Figure 2.1 Scheme of the experimental setup used for gaseous and solid fuels.

pressure drop over the bed in order to determine if the bed was fluidized or not. The exiting gas stream from the reactor was led into a condenser to remove the water. The composition and flow rate of the dry gas was determined on a volumetric base by an analyzer (Rosemount NGA-2000) which measured the concentrations of O_2, CO_2, CO, CH_4 and H_2. The schematic of the experimental setup is shown in Figure 2.1. For experiments using methane as fuel (papers I and II), the solid fuel injection and the sweeping gas parts were removed from the system.

In paper I, the reactivity and feasibility of the four oxygen carriers shown in Table 1 for CLC and CLOU processes are investigated. Their chemical-looping characteristics were evaluated at 900 and 925°C under alternating reducing (methane and nitrogen) and oxidizing conditions (5% O_2). Tendencies towards agglomeration, defluidization and loss of active phase were analyzed by changing the experimental process variables, such as reaction time, temperature and reducing and inert environments.

In paper II, a more in-depth investigation of $CuAl_2O_4$ (C4A-1050) oxygen carrier was carried out, in view of its high reactivity and fragmentation resistance observed in paper I. In addition, analysis of the phase relationship in the Cu−Al−O system during the redox cycle was carried out through step-wise sequential reduction with methane and re-oxidation in different oxygen concentrations.

For reassessment of the standard enthalpy of formation, ΔH_f^0, of $CuAl_2O_4$ in paper III, simultaneous thermogravimetry and differential scanning calorimetry (TGA/DSC; STA 409 PC *Luxx*) was performed. To achieve complete reduction of $CuAl_2O_4$, different masses of the
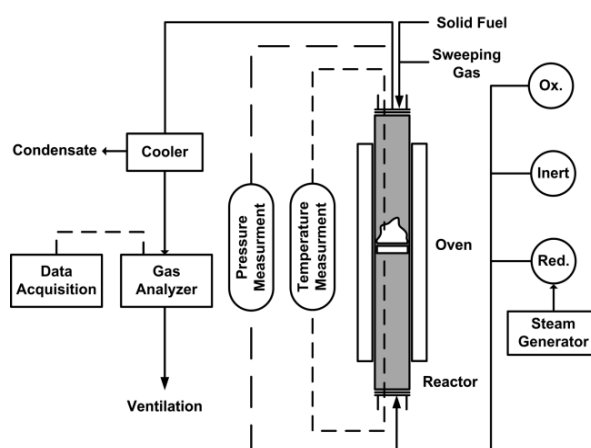
sample were exposed to a stream of 20% CO in Ar at 900°C. The enthalpy of reaction of $CuAl_2O_4$ with CO is obtained by integration of the area under the DSC curve. With this and the purity of the $CuAl_2O_4$ phase obtained from the average mass loss of the sample during reduction, the standard enthalpy of formation, ΔH_f^0, of $CuAl_2O_4$ could be determined.

In paper IV, the oxygen release and oxidation rates of the $MgAl_2O_4$-supported CuO oxygen carrier (C4MA-950) were investigated for the CLOU process in the temperature range 850–900°C and in the same setup as in papers I and II. This was done in view of its stable chemical-looping properties and absence of interaction between the active phase (CuO) and the support phase ($MgAl_2O_4$), observed in paper I. In order to obtain the rate of release of oxygen from CuO for CLOU, the oxygen carrier has to be exposed to an oxygen-deficient environment at a suitable temperature to allow for the decomposition of CuO; reaction (1.5). However, when nitrogen is used to simulate such a condition, reaction (1.5) may approach the equilibrium oxygen concentration thus releasing oxygen at a limited rate. This rate may be slower than the actual rate in a real process, where the oxygen released will be consumed by a fuel. Therefore, such experimental approach would not readily yield the true rate of oxygen release since CuO decomposition is hindered by the equilibrium concentration of oxygen surrounding the particles. Instead, the rate of oxygen release was obtained using a devolatilized wood char, sized 180–250 μm, as fuel. The reactor was fluidized with inert N_2, thus eliminating possible side reactions through gasification, and the released oxygen reacts directly with the char, keeping the ambient O_2 concentration low. In order to obtain the oxidation rate, the oxygen carrier was first reduced in inert nitrogen until the oxygen concentration at the outlet diminished. Subsequently oxidation was carried out in a flow of 5% O_2.

For further details of the experimental procedures respective to different investigations, see papers I–IV.

2.3   *Data Evaluation*

Using methane as fuel (papers I and II), the reactivity of the given oxygen carrier is quantified in terms of gas yield or conversion efficiency, γ. This is defined as the fraction of fully oxidized carbon fuel divided by the carbon containing gases in outlet stream, i.e. CO_2, CO and CH_4.

$$\gamma = \frac{y_{CO_2}}{y_{CO_2}+y_{CH_4}+y_{CO}} \tag{2.1}$$

Here y_i denotes the concentration (vol. %) of the respective gas, obtained from the gas analyzer.

The mass-based conversion of the oxygen carrier, ω, is defined as:

$$\omega = \frac{m}{m_{ox}} \qquad (2.2)$$

where m_{ox} is the mass of the oxygen carrier in fully oxidized state and m is the actual mass of the oxygen carrier during the experiments.

Equation (2.3) is employed for calculating ω as a function of time during the reduction period from the measured concentrations of various gaseous species in the gas analyzer:

$$\omega_i = \omega_{i-1} - \int_{t_0}^{t_1} \frac{\dot{n}_{out} M_o}{m_{ox}} \left(4y_{CO_2} + 3y_{CO} + 2y_{O_2} - y_{H_2} \right) dt \qquad (2.3)$$

where ω_i is the instantaneous mass-based conversion at time i, ω_{i-1} the mass-based conversion in the preceding instant, t_0 and t_1 the initial and final time of measurement, M_o the molar mass of oxygen, and $\dot{n}_{out}$ the molar flow rate of dry gas at the reactor outlet as measured by the analyzer.

In order to account for the effect of back-mixing of gases in CLOU experiments (paper IV), the reactor's effluent concentrations were deconvoluted assuming a first-order response of the analyzer. For this, the actual concentration of CO_2 and O_2 were approximated as follows

$$y_{i,act} = y_i + \tau \frac{dy_i}{dt} \qquad (2.4)$$

Here, $y_{i,act}$ is the deconvoluted concentration of the respective gas and τ is a time constant obtained as 1.2 s. The value of τ was determined by fitting the deconvolution equation to the change in O_2 concentration with time, when the fluidizing gas was changed from 10% O_2 to N_2 during reduction.

It was possible to measure the flow rate at the outlet of the reactor from the analyzer. However, the increase of flow rate due to large and instantaneous expansion of the gas during the conversion of the solid fuel in the reduction phase does not coincide with the peak concentration of the CO_2. This is because flow variations caused by reactions are measured instantly, while gas concentrations are measured with some time delay. Therefore for determination of the rate of decomposition of the CuO in the oxygen carrier, the corrected flow rate at the outlet of the reactor was calculated using mass balance over the reactor

system by the inlet flow rate, $\dot{n}_{in}$, and the deconvoluted concentration of the respective outgoing gas, $y_{i,act}$:

$$\dot{n}_{out,corr} = \frac{\dot{n}_{in}}{1 - y_{CO_2,act} - y_{O_2,act}} \tag{2.5}$$

Here, $\dot{n}_{in}$ is the sum of the flow rates from the bottom and the sweeping gas from the top of the reactor. For oxidation however, the flow rate used was the same as measured by the analyzer, $\dot{n}_{out}$, and no deconvolution was made.

In order to calculate the conversion of the oxygen carrier in CLOU experiments (paper IV), X_{red} and X_{ox} were defined, respectively during reduction, eq. (2.6), and oxidation, eq. (2.7)

$$X_{red} = \int_{t_0}^{t_1} \frac{\dot{n}_{out,corr}}{n_o} \left(y_{CO_2,act} + y_{O_2,act} \right) dt \tag{2.6}$$

$$X_{ox} = \int_{t_0}^{t_1} \frac{1}{n_o} \left(\dot{n}_{in} y_{O_2,in} - \dot{n}_{out} y_{O_2,out} \right) dt \tag{2.7}$$

n_o is the number of moles of molecular oxygen in the oxygen carrier that can be released through reaction (1.5).

Additional details of the data analysis and evaluation procedure respective to different investigations are given in papers I–IV.

3   RESULTS

3.1   *Oxygen Release from the Oxygen Carriers (Paper I)*

Figure 3.1 shows the oxygen concentration during an inert gas period for all samples. During this period, CuO decomposes spontaneously into Cu_2O via reaction (1.5) in the environment of inert nitrogen, thus the particles release oxygen. The oxygen concentration is relatively consistent with the theoretical equilibrium partial pressure, P_{O_2}, corresponding to the decomposition of CuO into Cu_2O, i.e. 1.5% and 2.7%, respectively at 900 and 925°C as shown in Table 1.1, for all the carriers tested except C4A-1050.

Figure 3.1 Oxygen concentrations of C4A and C4MA oxygen carriers during inert cycles at 900 and 925°C.

As opposed to the C4A-950 particles, the C4A-1050 sample has much less of gaseous oxygen release (CLOU) ability. The insignificant oxygen released from C4A-1050 (0.2 %), is further corroborated by the experiments with sand particles, also included in Figure 3.1 under identical experimental conditions. The only difference between the C4A-950 and C4A-1050 samples is the temperature at which they were calcined. Yet, while C4A-950 maintains the anticipated equilibrium oxygen concentration at both operating temperatures, C4A-1050 only releases oxygen to a minor extent.

From Table 2.1, it can be seen that in the C4A-1050 sample, $CuAl_2O_4$ is the predominant phase, while this is only a minor phase in the sample calcined at the lower temperature (950°C). In the fresh sample, CuO which is capable of releasing oxygen at above 850°C,[16] appears as a minor phase together with excess and unreacted alumina. Thus in this case, very little oxygen is released via the CLOU mechanism since $CuAl_2O_4$ is quite incapable of releasing oxygen. The insignificant release of oxygen from the C4A-1050 sample is investigated in more detail in Section 3.5. For C4MA-950 and C4MA-1050 samples however, an identical equilibrium concentration of oxygen release is obtained irrespective of the calcination temperature.
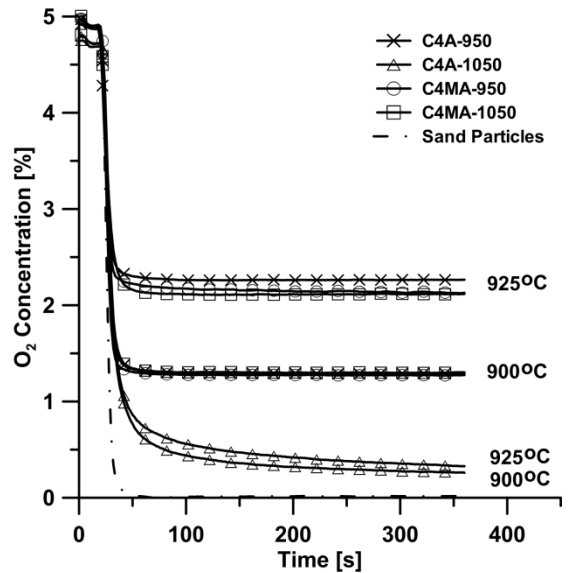
3.2   Reactivity of the Oxygen Carriers (Papers I and II)

Following the inert gas cycles, successful cycles of oxidation and reduction were carried out for all oxygen carriers. Figure 3.2 shows the concentration profiles for the C4A-950 sample for the 20 s reduction cycle at 900°C using methane as fuel. The decomposition of CuO during the short interval in inert gas prior to fuel injection is due to the spontaneous release of oxygen via the CLOU mechanism. The fuel (methane) reacts exothermically with the released oxygen, producing CO_2 and H_2O, with concomitant
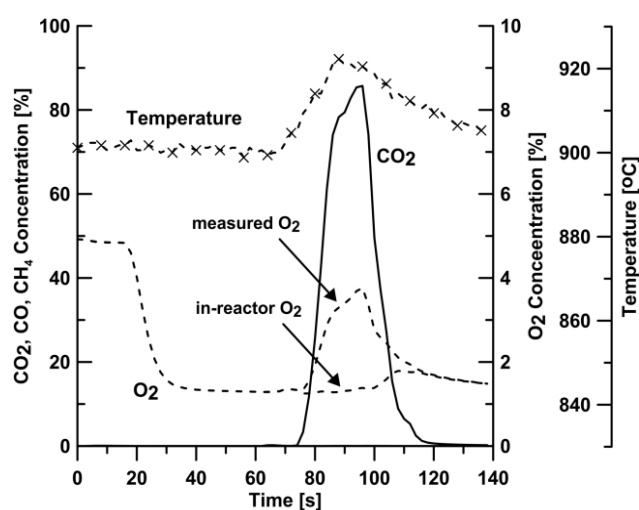

Figure 3.2 Concentration and temperature profiles for C4A-950 during reduction cycle at 900°C.

increase in temperature due to the overall exothermic nature of the reactions; this is common for copper-based oxygen carriers.[11] The rise in temperature should raise the equilibrium oxygen concentration, although this is not observed in Figure 3.2, likely due to fast reaction of methane with any excess of released oxygen. It is also evident that the oxygen concentration in the reactor is considerably lower due to diluting effect of steam.

Table 3.1 summarizes the results from the reactivity test of the investigated oxygen carriers. The carriers lose approximately 3% of their mass as they are converted during 20 s of reduction with methane (ω going from 1 to 0.97). During the oxidation cycle that follows, the carrier is expected to retrieve this amount of oxygen, meaning that ω must revert from 0.97 to 1. Only then, a truly reversible redox behavior of the carrier could be anticipated. The incomplete recovery of $\Delta\omega$ in case of C4A-950 and C4A-1050 indicates that part of the active phase (CuO and $CuAl_2O_4$, respectively; Table 2.1) is not retrieved. However, for the C4MA, the carriers recovered almost the expected mass-based conversion, irrespective of the calcination temperature. This shows that the active CuO phase has remained intact when $MgAl_2O_4$ is used as support.

Under the experimental conditions employed, the theoretical change in mass-based conversion, $\Delta\omega$, of CuO to Cu at the end of reduction with methane for 70 s should be 8%. As shown in Table 3.1, this was essentially obtained in the case of C4MA particles with full

conversion of methane. Reduction times longer than 70 s did not increase the conversion any further for either of the two carriers, confirming that the limit of CuO reduction is reached. On the contrary, in the case of C4A-950 and C4A-1050 the change in ω was less. This was associated with incomplete methane conversion during the latter part of the reduction period.

Table 3.1 Summary of reactivity test for the oxygen carriers.

	C4A-950	C4A-1050	C4MA-950	C4MA-1050
CH$_4$ for 20 s (900°C)				
Gas conversion [-]	Complete, $\gamma = 1$			
Oxygen carrier conversion during reduction [%]	$\Delta\omega = 3$			
Oxygen carrier conversion during oxidation [%]	$\Delta\omega = 1$		$\Delta\omega = 3$	$\Delta\omega = 2.5$
CH$_4$ for 70 s (925°C)				
Gas conversion [-]	Incomplete, $\gamma < 1$		Complete, $\gamma = 1$	
Oxygen carrier conversion during reduction [%]	$\Delta\omega = 4$		$\Delta\omega = 8$	
Oxygen carrier reversibility	Partially reversible		Reversible	
State of CuO active phase	Not intact	N/A	Intact	

It is reported that the diffusion of O$_2$ in the depleted oxygen carrier during the oxidation cycle could be hindered by the CuO layer partially surrounding the reduced Cu$_2$O and Cu grains.[44, 47, 48] Therefore the incomplete oxidation of C4A-950 could initially be connected with this resistance. However, the XRD patterns extracted at the end of experiment for C4A-950 only indicated the oxidized state of the oxygen carrier (i.e. only CuO) together with an increase in the content of CuAl$_2$O$_4$ and CuAlO$_2$ (see paper I). Similarly, the C4A-1050 sample could not be completely oxidized, although it did not contain a significant amount of CuO in the fresh state. Moreover, the complete regain of ω in oxidation for the C4MA samples indicates that the oxidation of Cu$_2$O to CuO in previous cycles was not subject to any resistance towards O$_2$ diffusion in the depleted CuO layer as suggested previously.[44, 47, 48] Thus as will be shown in the phase analysis later (Section 3.5), the remaining deficiency in $\Delta\omega$ for the case of C4A samples can be attributed to the fact that a part of the active phase (CuO or CuAl$_2$O$_4$) is bound in the form of a ternary compound (CuAlO$_2$), that is not readily converted back to the initial composition of the oxygen carrier upon oxidation.

3.3 Physical Aspects of the Oxygen Carriers under Redox Cycle (Papers I and II)

It is important to examine the integrity of particles for possible occurrence of fragmentation and/or agglomeration after reactivity testing. The post-reaction ESEM images of all samples after the reactivity test are shown in Figure 3.3 (a-d). Compared to the fresh sample, the surface morphology of the C4A-1050 and C4MA-950 particles did not change appreciably. For the C4MA-1050 sample, most of the particles disintegrated forming a considerable amount of fines. The used C4A-950 particles also exhibited slight fragmentation.
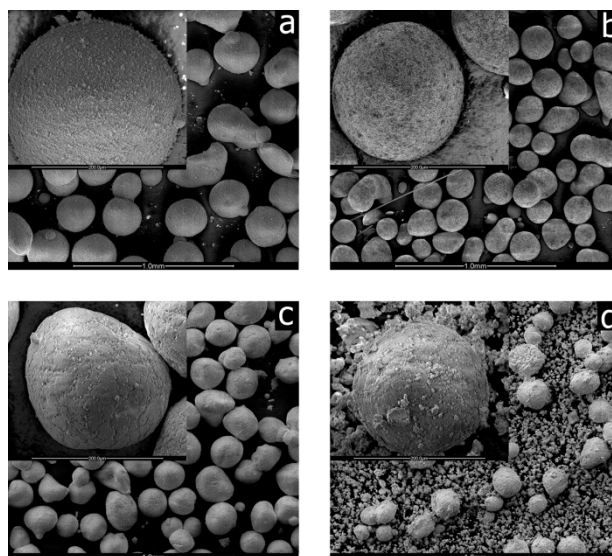

Figure 3.3 ESEM images of (a) C4A-950, (b) C4A-1050, (c) C4MA-950 and (d) C4MA-1050 after reactivity test. The micrometer bars in the inset and outset images are 200 μm and 1 mm, respectively.

In paper II, the C4A-1050 sample was exposed to more redox cycles (45 reduction cycles with methane). At 900 and 925°C, the particles maintained their integrity since fragmentation and agglomeration of the particles could not be observed. For detailed results on the changes in apparent density, BET and particle size distribution (PSD) of the oxygen carriers, see papers I and II.

3.4 Standard Enthalpy of Formation, ΔH_f^0, of $CuAl_2O_4$ (Paper III)

There is a discrepancy in the standard enthalpy of formation, ΔH_f^0 (at 25°C), of $CuAl_2O_4$ between the Landolt-Börnstein[49] and Knacke et al.[50] databases (−1946.81 vs. −1813.33 kJ mol⁻¹, respectively). As a result of this inconsistency, the calculated phase equilibira and enthalpy of reaction, ΔH, of $CuAl_2O_4$ with reducing gases varies significantly. For instance, Adanez et al.[15] calculated the standard enthalpy of reaction, ΔH^0, of $CuAl_2O_4$ with methane at 25°C as endothermic (282.2 kJ mol⁻¹), based on data similar to Landolt-Börnstein.[49] However, the experiments in papers I and II for reduction of $CuAl_2O_4$ with methane at 900–950°C have instead shown a strongly exothermic reaction and the standard reaction enthalpy, ΔH^0, at 25°C was calculated as −252.0 kJ mol⁻¹, based on data of Knacke et al.[50] Thus, the standard enthalpy of formation, ΔH_f^0, of $CuAl_2O_4$ requires reassessment. In paper III, this is carried out

by means of thermogravimetry and differential scanning calorimetric (TGA/DSC) analysis using the reaction enthalpy, ΔH, of $CuAl_2O_4$ with CO. The results are also compared with those obtained from standard Gibbs free energy data, ΔG^0, reported by Jacob and Alcock[51] and Gadalla and White.[52]

Figure 3.4 shows the TG and DSC curves for the reduction of $CuAl_2O_4$ sample at 900°C and for two runs. The average mass loss is approximately 7.6 wt. % corresponding to the reduction of $CuAl_2O_4$ in the sample to Cu and Al_2O_3. Thus, accounting for the purity of the $CuAl_2O_4$ phase in the sample (86 wt. %), the enthalpy of reaction, ΔH, of $CuAl_2O_4$ with CO at 900°C can be estimated as –149.0±7.6 kJ mol^{-1}. Using Hess's law and formation enthalpies of CO, CO_2, Cu and Al_2O_3 at 900°C, in addition to the heat capacities of each component,[49, 50] the corresponding average of the standard enthalpy of formation, ΔH_f^0, of $CuAl_2O_4$ at 25°C is determined as –1829.9±7.6 kJ mol^{-1}. This value is in good agreement with the corresponding value reported in the thermodynamic database by Knacke et al.[50]

The standard enthalpy of reaction, ΔH^0 (at 25°C), of $CuAl_2O_4$ with CO obtained here (–128.75 kJ mol^{-1}) is also in agreement with the corresponding value obtained when using the ΔG^0 data by Jacob and Alcock[51] (see paper III for more details). Thus, for $CuAl_2O_4$, the thermodynamic data in studies[50, 51] are more reliable and are used in the development of phase relationships of the Cu–Al–O system in Section 3.5.
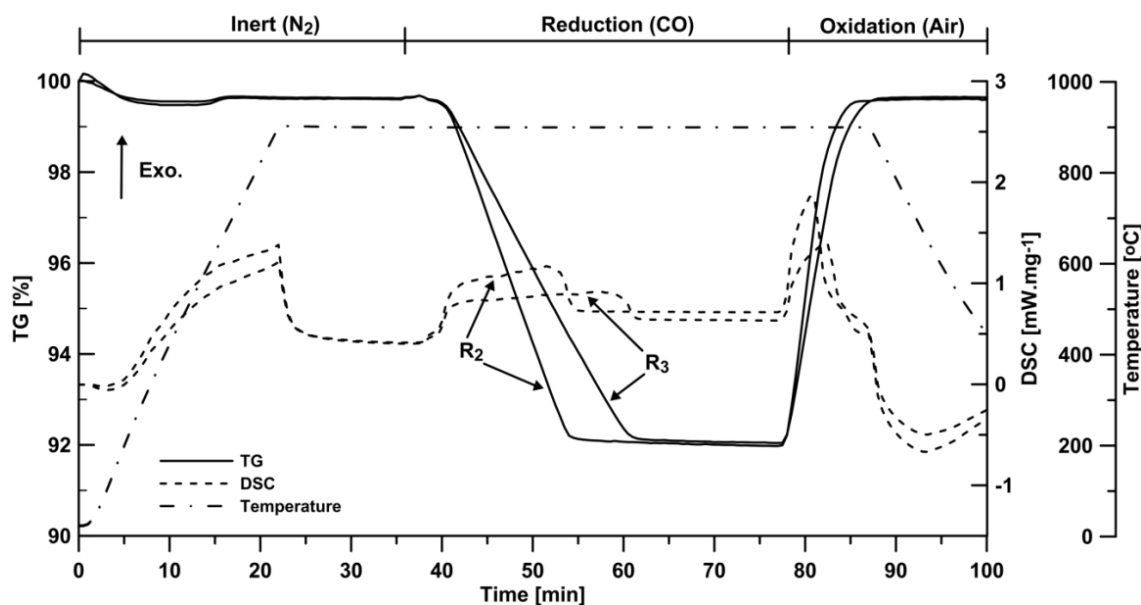

Figure 3.4 TG and DSC curves of CuAl$_2$O$_4$ heated in N$_2$ to 900°C at 40°C min^{-1}, followed by isothermal reduction in CO and subsequent oxidation in air for two runs (R$_2$ and R$_3$). The gas flow rate in all phases was maintained at 50 mL$_N$ min^{-1}.

3.5   Phase Analysis of the Cu–Al–O system during Redox Cycle (Papers I and II)

The relationship among various phases in the pseudobinary CuO–Al_2O_3 system is of great relevance to the use of Al_2O_3-supported CuO as oxygen carrier in the CLC process. Of importance is the formation of $CuAl_2O_4$ spinel during calcination of the oxygen carrier at high temperatures (around 900–1000°C)[53-56] as per the reaction:

$$CuO + Al_2O_3 \rightarrow CuAl_2O_4 \qquad (3.1)$$
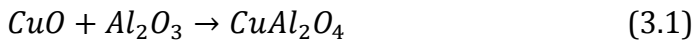
As a result of chemical-looping process, the phase field in the Cu–Al–O system is dependent on the oxygen partial pressure during the redox cycle in the temperature range of relevance. Figure 3.5 shows the equilibrium phase relationships at 1 atm. total pressure using the Gibbs free energy data reported by Jacob and Alcock.[51]

In the context of the envisaged application of $CuAl_2O_4$ as an oxygen carrier in continuous operation, other reactions in addition to those depicted in Figure 3.5 should be also considered. Consequently, Figure 3.6 shows a series of P_{O_2}-dependent reactions in the temperature range of interest to CLC at a total pressure of 1 atm. The equilibrium lines shown in Figure 3.6 were also based on the Gibbs energy data of Jacob and Alcock.[51]

Among these, of particular interest is the following reaction:

$$4CuAl_2O_4 \rightarrow 4CuAlO_2 + 2Al_2O_3 + O_2 \qquad (3.2)$$
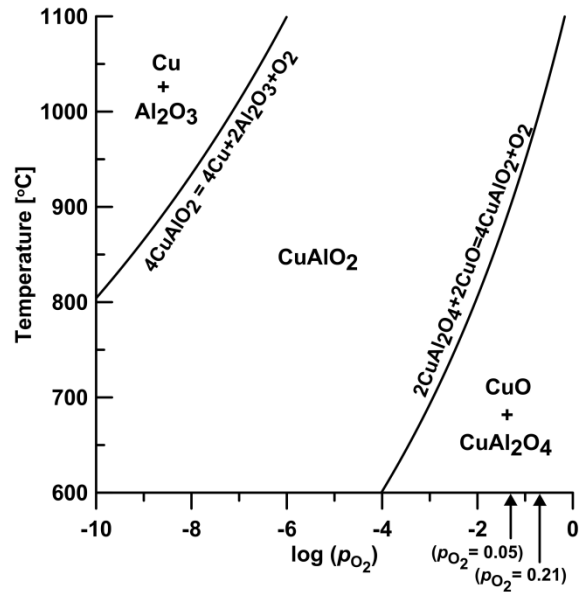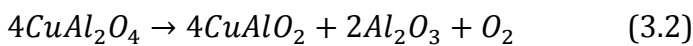

Figure 3.5 Equilibrium phase relationships in the ternary Cu–Al–O system in a 1:1 molar mixture of Cu and Al at 1 atm. total pressure based on the Gibbs energy data reported by Jacob and Alcock.[51]
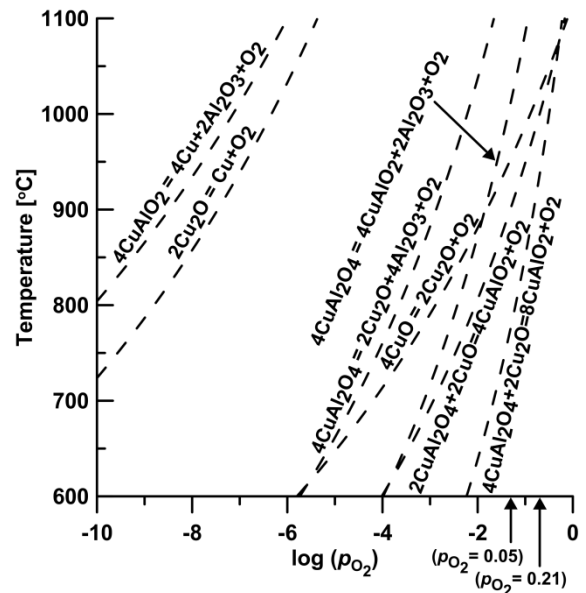

Figure 3.6 Possible P_{O_2}-dependent phase equilibria in the Cu–Al–O system at 1 atm. total pressure based on the Gibbs energy data reported by Jacob and Alcock.[51]

Reaction (3.2) indicates that $CuAl_2O_4$ could potentially be a CLOU material by releasing O_2, albeit at lower equilibrium partial pressure compared to that of $CuO–Cu_2O$ at temperatures above 900°C. Tsuboi et al.[57] reported that at 1050°C, $CuAl_2O_4$ undergoes reduction into $CuAlO_2$ in the case of thin copper films deposited on alumina substrate in a highly oxygen depleted vacuum. However, here it was observed that $CuAl_2O_4$ subjected to N_2-purge for 4 h at 900°C was incapable of releasing oxygen; no $CuAlO_2$ could be observed either (see paper I). On the other hand, it is well-established that $CuAl_2O_4$ could be reduced by methane or syngas.[22, 26, 28, 34, 45] Thermogravimetric and temperature programmed reduction (TPR) studies[34, 58-60] on bulk samples also corroborate this. Thus, the observation of Tsuboi et al.[57] could perhaps be explained on the basis of the higher temperature compared to this study and the ease with which thin film samples undergo dissociation, compared to bulk samples such as those investigated here.

In order to understand the reducing and oxidizing pathways in the Cu–Al–O system and analyze the reversibility of the phases during the redox process, the $CuAl_2O_4$ (C4A-1050) oxygen carrier was further investigated. Figure 3.7 shows the XRD pattern of $CuAl_2O_4$ subjected to isothermal step-wise reduction by methane at 900°C in a sequence of varying durations. In the sample reduced for the shortest duration (10 s), peaks belonging to Cu_2O appear. Longer (16 and 24 s) reduction is followed by the decrease in intensity (hence amount) of $CuAl_2O_4$ and increase in that of $CuAlO_2$ and Cu_2O. It should be pointed out that in paper I, Cu_2O was also seen during annealing in an inert environment, which was ascribed to the presence of small amount of unreacted CuO in the fresh sample. A similar explanation is valid in the experiments here. However, the increase in the amount of Cu_2O seen in
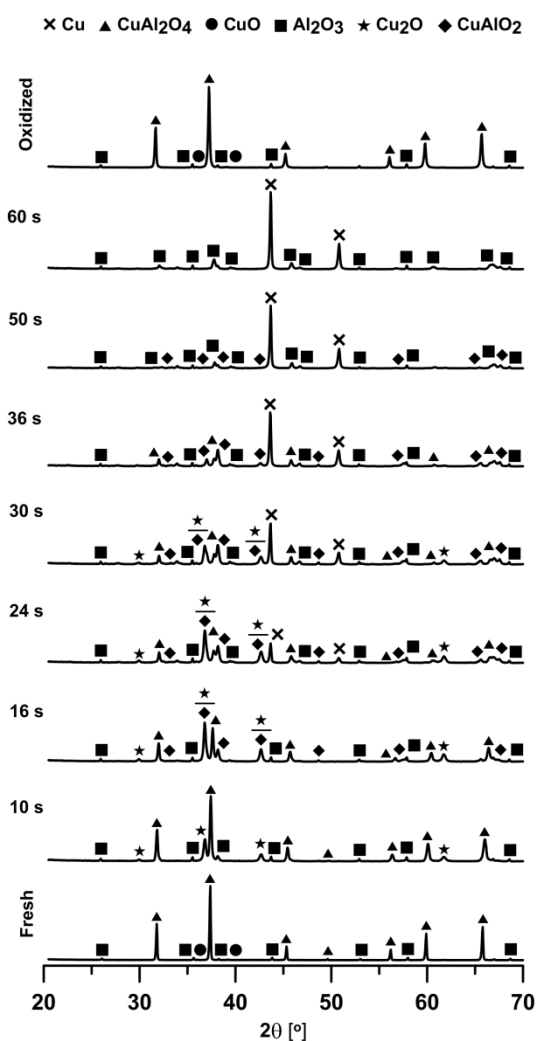

Figure 3.7 Systematic phase evolution in $CuAl_2O_4$ oxygen carrier reduced by methane at 900°C for 60 s; the topmost XRD pattern is for the oxygen carrier oxidized in 10% O_2 stream after being reduced for 60 s with methane.

the diffraction patterns at 16 and 24 s in Figure 3.7, suggests that Cu_2O is not only formed from remnant CuO in the $CuAl_2O_4$ oxygen carrier. Using TPR, Patrick et al.[59, 60] showed that the reduction of $CuAl_2O_4$ catalyst proceeds by the simultaneous formation of $CuAlO_2$ and Cu_2O via reactions (3.2) and (3.3), respectively.

$$4CuAl_2O_4 \rightarrow 2Cu_2O + 4Al_2O_3 + O_2 \qquad (3.3)$$

The formation and increase of $CuAlO_2$ and Cu_2O via reactions (3.2) and (3.3), respectively, after 16 and 24 s in Figure 3.7 is also in agreement with the P_{O_2}-dependency shown in Figure 3.6, given the highly reducing environment created by methane. In the sample reduced for 24 s, the onset of formation of elemental Cu is clearly detected. The copper concentration increases with time of reduction, as is evident from all of the diffraction patterns at $t \geq 24$ s. In case of reduction carried out for more than 36 s, the XRD pattern contains peaks for alumina and elemental copper with traces of delafossite ($CuAlO_2$). In samples reduced for 60 s, only metallic copper and alumina are present. This again is in complete conformity with Figure 3.5 in regard to the ultimate reduction of $CuAl_2O_4$ to Cu and Al_2O_3 as also reported elsewhere.[60, 61] Thus, the oxygen carrier is completely reduced by methane in 60 s. The intensity of the α-Al_2O_3 should increase during the consecutive reduction steps as it is released from the $CuAl_2O_4$, however, this is not observed in Figure 3.6. A possible explanation for this may be that the alumina is still covered with the copper layer. The original phases ($CuAl_2O_4$ and Al_2O_3) are fully restored upon oxidation in 10% O_2 as seen from the topmost XRD pattern in Figure 3.6.

From the foregoing discussion and the reactivity test presented in Sections 3.2 and 3.3, it is apparent that the $CuAl_2O_4$ spinel functions well as an oxygen carrier. However, in a realistic CLC unit, the oxygen carrier is only partially reduced in order to avoid unconverted CH_4, CO and H_2. Recently, Kumekawa et al.[62] showed that $CuAlO_2$ is thermodynamically stable in air above 900–1000°C, which agrees reasonably with Figure 3.5 and 3.6. However, below this temperature range, $CuAlO_2$ undergoes the following kinetically hindered reactions[33, 36, 39]

$$4CuAlO_2 + O_2 \rightarrow 2CuO + 2CuAl_2O_4 \qquad (3.4)$$

$$8CuAlO_2 + O_2 \rightarrow 2Cu_2O + 4CuAl_2O_4 \qquad (3.5)$$

To investigate the kinetic aspect of reactions (3.4) and (3.5), oxygen carrier samples from the reactivity test consisting of alternating reduction (with methane) and oxidation at 900°C, albeit with shorter reduction span (20 s) similar to that explained in Section 3.2, were used.

Here, 1 g of the used sample (oxidized), which contained a considerable fraction of CuAlO$_2$, was reoxidized in consecutive steps of 30 min. in streams containing 5, 10, 15 and 21% O$_2$ at 900°C. Figure 3.8 shows the phase evolution in each of the re-oxidation steps. To begin with, the oxidized sample from the reactivity test with shorter reduction span (20 s; methane) contains a 3-phase mixture of CuAl$_2$O$_4$, CuAlO$_2$ and Al$_2$O$_3$. As is evident from the figure, CuAlO$_2$ persists under several re-oxidation attempts, indicating that the oxidation of CuAlO$_2$ according to reaction (3.4) and/or (3.5) is kinetically hindered. This is further exemplified by the fact that complete conversion of the delafossite phase into the parent spinel (CuAl$_2$O$_4$) is realized only after extended oxidation in air (P_{O_2} = 21%) at 900°C for an additional 1 h, i.e. a total of 3 h in varying oxygen concentrations. The increase of CuO amount in the fully re-oxidized sample (topmost XRD pattern in Figure 3.8) compared to the fresh oxygen carrier (bottommost XRD pattern in Figure 3.7), is in agreement with reaction (3.4). It should be noted that in an actual CLC unit, air is used for the oxidation of the depleted carrier; however the oxygen concentration at the outlet of the air reactor is much lower than 21%. Therefore part of the CuAlO$_2$ phase resists oxidation.
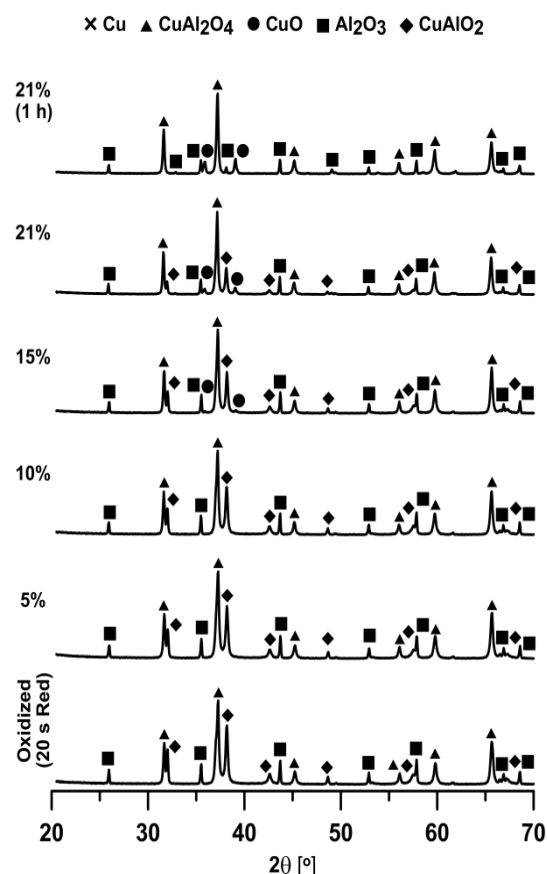
Figure 3.8 Systematic phase evolution in CuAl$_2$O$_4$ oxygen carrier during re-oxidation for 30 min. in P_{O_2} = 5, 10, 15 and 21% O$_2$ streams at 900°C; the bottommost XRD pattern is for the oxidized sample from the reactivity test with shorter reduction span (20 s; methane); the topmost XRD pattern is for the sample re-oxidized in air (21% O$_2$) for an additional 1 h.

3.6 *Rate of Oxygen Release of the CuO/MgAl$_2$O$_4$ Oxygen Carrier for CLOU (Paper IV)*

In Section 3.2, it was observed that the MgAl$_2$O$_4$-supported CuO oxygen carrier showed stable chemical-looping properties during seventeen cycles of redox using methane as fuel and 5% O$_2$ in N$_2$. Thus in paper IV, an attempt was made to obtain the oxygen release and oxidation rates of this oxygen carrier for the CLOU process. The experiments were designed in a way to

avoid the oxygen equilibrium restriction and obtain a relevant rate of oxygen release as described in Section 2.2.

Figure 3.9 shows the conversion of the oxygen carrier as a function of time during reduction, X_{red}, in the temperature range of 850–900°C. The 30 s span before the introduction of the devolatilized wood char during reduction of the oxygen carrier shown in Figure 3.9 is to allow the conditions in the reactor to reach close to equilibrium oxygen concentration and avoid back-mixing from the previous oxidation. It is clear that the conversion of the oxygen carrier is slow during this time due to the conditions in the reactor being close to thermodynamic equilibrium because of the oxygen released. Upon insertion of the fuel, the oxygen surrounding the oxygen carrier is removed almost immediately. Thus the oxygen carrier releases the remaining oxygen at the maximum rate possible. This results in the sudden increase in the rate of conversion of the oxygen carrier. The oxygen carrier is completely reduced to Cu_2O at 900°C. At lower temperatures however, the initial rate of reaction seems to be slower, as seen from the slope of the plots in Figure 3.9, and hence the conversion, X_{red}, has not reached unity at the end of the reduction period.

In order to model the oxygen release, i.e. the decomposition of CuO to Cu_2O shown in reaction (1.5), it was assumed that the experiments are conducted within the kinetically controlled regime, given oxygen being efficiently consumed by the devolatilized wood char. For details of the
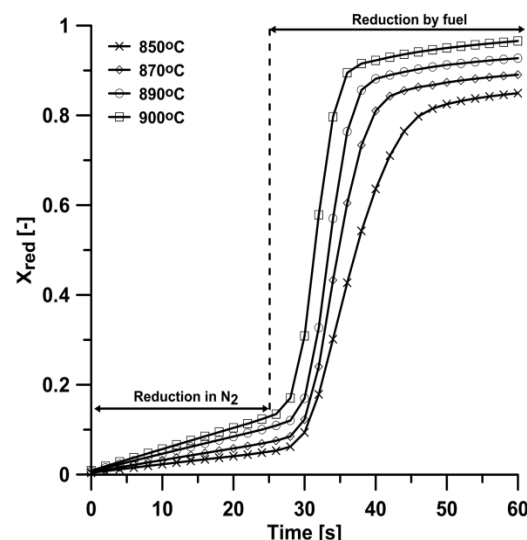
Figure 3.9 Oxygen carrier conversion during oxygen release (reduction) period, X_{red}, as a function of time for 1 g of $CuO/MgAl_2O_4$ in 10 g of quartz in the temperature range of 850–900°C using 0.1 g of devolatilized wood char.
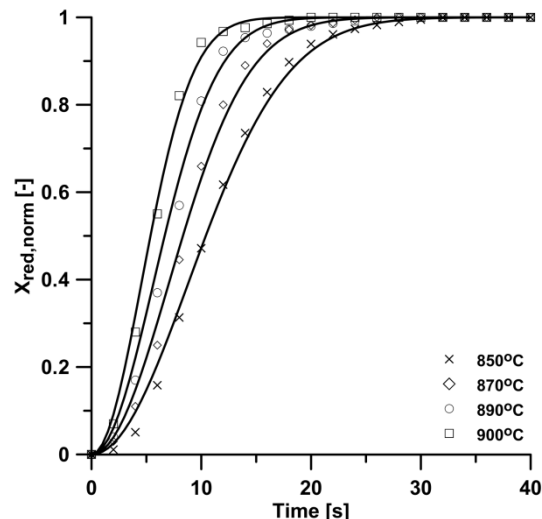

Figure 3.10 Normalized oxygen carrier conversion during oxygen release (reduction) cycle, $X_{red,norm}$, as a function of time and fitting of the Avrami-Erofeev model for 1 g of $CuO/MgAl_2O_4$ in 10 g of quartz in the temperature range of 850–900°C using 0.1 g of devolatilized wood char.

implication of such assumption and their validation, see paper IV. To determine which kinetic model best describes the progress of reaction (1.5), common gas-solid reaction kinetic models were fit to the conversion, X_{red}, versus time data in Figure 3.9, including reaction order models, nucleation models, diffusion models and geometrical contraction models.[63] The results of different kinetic models fitting are presented in paper IV. Of all the investigated models, the Avrami-Erofeev mechanism assuming two-dimensional nuclei growth (n = 2) was found to describe the decomposition reaction best, with coefficient of variance, R^2, of approximately 0.986. The rate equation for such a reaction model can be written as

$$\frac{dX_{red,norm}}{dt} = k_r 2\left(1 - X_{red,norm}\right)\left[-ln\left(1 - X_{red,norm}\right)\right]^{\frac{1}{2}} \tag{3.6}$$

where k_r is the rate constant of the forward reaction in eq. (1.5). $X_{red,norm}$ is the normalized measured conversion of the oxygen carrier shown in Figure 3.9, X_{red}, to obtain full conversion of the carrier. Figure 3.10 shows the results of modelling the oxygen carrier conversion during oxygen release (reduction) using this model. The sigmoidal shape of the oxygen carrier conversion, $X_{red,norm}$, as function of time shown in Figure 3.10 also indicates that the decomposition reaction, eq. (1.5), proceeds via nucleation and nuclei growth.[63] Similar results have also been found for gas-solid reactions of CuO oxygen carriers[45, 64] and decomposition of pure CuO powder.[44]

3.7 *Rate of Oxidation of the CuO/MgAl$_2$O$_4$ Oxygen Carrier for CLOU (Paper IV)*

Figure 3.11 shows the derivative of the conversion of the oxygen carrier during oxidation, $\frac{dX_{ox}}{dt}$, and the partial pressure of oxygen at the reactor's outlet, with respect to the oxygen carrier conversion, X_{ox}. Here, it can be seen that at any conversion degree, the derivative (reaction rate) is limited by the equilibrium oxygen concentration at the respective reaction temperature. Thus, the rapid oxidation reaction at all temperatures makes it difficult to obtain the rate of oxidation of Cu$_2$O to CuO. As the oxygen carrier is exposed to a partial pressure of oxygen, the apparent rate equation during oxidation, assuming first-order dependency on a logarithmic average of oxygen concentration can be written as

$$\frac{dX_{ox}}{dt} = k_{-r} P_{O_2,ave} \tag{3.7}$$

Here, $P_{O_2,ave}$ is based on the difference between actual oxygen concentration and the equilibrium oxygen concentration. Thus, the $P_{O_2,ave}$ can be calculated as per eq. (3.8),

$$P_{O_2,ave} = \frac{P_{O_2,in} - P_{O_2,out}}{ln(P_{O_2,in} - P_{O_2,eq}/P_{O_2,out} - P_{O_2,eq})} \qquad (3.8)$$

However, due to the fast oxidation reaction, the outlet partial pressure of oxygen is equal to equilibrium oxygen concentration at the respective temperature (Figure 3.11). This will give a value of $P_{O_2,ave}$ of zero, and consequently k_{-r} will be infinite. Therefore, it is not possible to calculate a meaningful rate constant, k_{-r}, using eqs. (3.7) and (3.8). In order to obtain a "minimum value" of rate constant for the experiments in this work, an oxygen concentration of 1% is assumed at the outlet of the reactor in eq. (3.8). As an example, the logarithmic average of oxygen partial pressure, $P_{O_2,ave}$, is approximately 1.82% at 850°C assuming 5% O_2 at the inlet and 1% O_2 at the outlet of the air
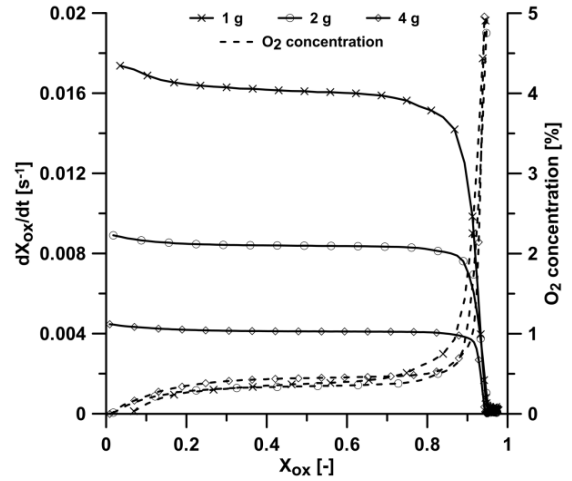

Figure 3.11 Oxygen carrier conversion derivative during oxidation cycle, $\frac{dX_{ox}}{dt}$, and the oxygen concentration at the outlet of the reactor (not deconvoluted), as a function of oxygen carrier conversion, X_{ox}, for 1, 2 and 4 g of oxygen carrier in 10 g of quartz at 850°C in 5% O_2 stream.

reactor. Therefore, using the corresponding value for $\frac{dX_{ox}}{dt}$ in Figure 3.11, the minimum k_{-r} is estimated to be 0.89 s^{-1} atm^{-1} at 850°C.

3.8 Solids Circulation Rate and Inventory of the CuO/MgAl₂O₄ Oxygen Carrier for CLOU (Paper IV)

Using the reactions rates, k_r and k_{-r}, obtained in Sections 3.6 and 3.7, the amount of solids inventory needed for the CLOU process using the CuO/MgAl$_2$O$_4$ (C4MA-950) oxygen carrier can be calculated. An oxygen carrier mass-based conversion difference, $\Delta\omega$, of 1–2% results in a recirculation rate of solids, $\dot{m}_{OC}$, between 4–8 kg s^{-1} MW$_{th}^{-1}$ for 1 MW$_{th}$ assuming carbon as fuel with a lower heating value (LHV) of 32.8 MJ kg^{-1}.[8] This is also within the feasible range in a system of reactors similar to CFB boilers.[65] For details of the calculation method of the solids circulation rate and inventory, see paper IV. Additionally, negligible mass transfer resistance between the bubbles and emulsion phase in the fluidized-bed reactor and a first-order oxidation reaction with respect to oxygen concentration are assumed. Temperatures of 900 and 850°C are assumed for the fuel and the air reactor, respectively. Thus, the solids needed per MW$_{th}$ in the fuel and the air reactor varies between, 30–60 and 43–87 kg MW$_{th}^{-1}$,

respectively, giving a total of 73–147 kg MW_{th}^{-1}. The required solids inventory in the fuel reactor obtained here is lower than previously reported investigations for a 40 wt. % CuO on ZrO_2 support using petcoke as fuel (120–200 kg MW_{th}^{-1})[39] and recent studies in continuous operation using a spray-dried 60 wt. % CuO on $MgAl_2O_4$ support (235 kg MW_{th}^{-1} at 960ºC),[27] but is in close agreement with the values obtained by Adánez-Rubio et al.[66] for the spray-dried 60 wt.% CuO on $MgAl_2O_4$ support (39 kg MW_{th}^{-1} at 930ºC).

4 CONCLUSIONS

In the first part of this work, the feasibility of four oxygen carriers consisting of CuO supported on Al_2O_3 and $MgAl_2O_4$ for CLC and CLOU processes were investigated. Their chemical-looping performance was examined in a laboratory-scale fluidized-bed reactor at 900 and 925°C under alternating reducing and oxidizing conditions. The main conclusions from this part of the work were:

- All oxygen carriers showed complete conversion of methane during short reduction cycles. Moreover, three out of four oxygen carriers featured the rapid release of oxygen in an inert environment (CLOU).

- In the case of Al_2O_3 as support, the CuO reacted with Al_2O_3, thus forming $CuAl_2O_4$, which is also a viable oxygen carrier, although it has no uncoupling properties. Furthermore, part of the CuO and $CuAl_2O_4$ active phases were not retrieved upon oxidation due to formation of $CuAlO_2$.

- During longer reduction cycles, the $MgAl_2O_4$-supported oxygen carriers showed that the active CuO phase is retained by avoiding the interaction between CuO and the support, thus offering stable oxygen release.

The $CuAl_2O_4$ oxygen carrier (C4A-1050) was further investigated in a larger number of cycles and in the temperature range of 900–950°C for CLC, concluding that:

- Agglomeration and/or defluidization were not encountered during experiments at 900 and 925°C. However, after reactivity testing at 950°C, soft agglomeration and particle fragmentation were observed.

In order to establish the phase relationships in the Cu–Al–O system, the standard enthalpy of formation, ΔH_f^0, of $CuAl_2O_4$ was reassessed using TGA/DSC due to a discrepancy between thermodynamic databases. Systematic phase analysis of the Cu–Al–O system during the redox cycle was carried out as a function of duration of reduction and oxygen concentration during the re-oxidation period. This revealed that:

- The reduction of the spinel ($CuAl_2O_4$) involves the formation of $CuAlO_2$, Cu_2O and

elemental Cu.

- The $CuAlO_2$ has slow kinetics for re-oxidation which results in partial loss of the active phase after several redox cycles. This likely decreases the oxygen ratio of the carrier; although, this may be compensated by a larger solids inventory.

The rate of oxygen release and the rate of oxidation of the $MgAl_2O_4$-supported CuO oxygen carrier (C4MA-950) were also investigated in the temperature range of 850–900°C for CLOU. Devolatilized wood char was added to facilitate oxygen release from the oxygen carrier in N_2-fluidization by maintaining low oxygen concentration around the particles. The Avrami-Erofeev mechanism was found best to model the rates of oxygen release. However, during oxidation it was observed that the rate is limited by oxygen supply, indicating rapid conversion of the oxygen carrier. Based on the obtained rates, the minimum solids inventory was also determined for a CLOU unit operating at a temperature of 900°C in the fuel reactor and 850°C in the air reactor. The total needed inventory of solids in the fuel and the air reactor was estimated to be between 73–147 kg MW_{th}^{-1}.

Although some of the oxygen carriers investigated in this work functioned well (e.g. $MgAl_2O_4$-supported CuO and $CuAl_2O_4$) with no sign of agglomeration and fragmentation, they likely need to be modified for use in continuous operation due to their low crushing strength (0.5 N). This in turn could affect the results; for instance, the reactivity of the oxygen carriers or the rates of oxygen release will likely change considerably. However, it should be noted that the methods developed and presented here are applicable to any other oxygen carrier.

NOMENCLATURE

γ	Gas yield or conversion efficiency [–]
y_i	Gas concentration of the i specie as measured by the analyzer [vol. %]
$y_{i,act}$	Deconvoluted gas concentration of the i specie [vol. %]
$\frac{dy_i}{dt}$	Change in gas concentration of the i specie over a time interval [vol. % s^{-1}]
ω	Mass-based conversion of the oxygen carrier [%]
$\Delta\omega$	Change in mass-based conversion of the oxygen carrier [–]
m_{ox}	Mass of the oxygen carrier in fully oxidized state [g]
m	Actual mass of the oxygen carrier during the experiments [g]
n_o	Number of moles of molecular oxygen in the oxygen carrier [–]
X_{red}	Conversion of the oxygen carrier during reduction [–]
X_{ox}	Conversion of the oxygen carrier during oxidation [–]
τ	Time constant [s]
$\frac{dX_{red}}{dt}$	Conversion rate of the oxygen carrier during reduction [s^{-1}]
$\frac{dX_{ox}}{dt}$	Conversion rate of the oxygen carrier during oxidation [s^{-1}]
$\dot{n}_{out}$	Molar flow rate of dry gas at the outlet of the reactor [mol s^{-1}]
$\dot{n}_{in}$	Molar flow rate at the inlet of the reactor [mol s^{-1}]
$\dot{n}_{out,corr}$	Corrected molar flow rate at the outlet of the reactor [mol s^{-1}]
t	Time [s]
M_o	Molar mass of oxygen [g mol^{-1}]
ΔH_f^0	Standard enthalpy of formation (at 25°C) [kJ mol^{-1}]
ΔH^0	Standard enthalpy of reaction (at 25°C) [kJ mol^{-1}]
ΔH	Enthalpy of reaction [kJ mol^{-1}]
ΔG^0	Standard Gibbs free energy [kJ mol^{-1}]

k_r	Rate constant during oxygen release (reduction) of CuO [s^{-1}]
$X_{red,norm}$	Normalized conversion of the oxygen carrier during reduction [–]
$\frac{dX_{red,norm}}{dt}$	Normalized conversion derivative of the oxygen carrier during reduction [s^{-1}]
k_{-r}	Rate constant during oxidation of Cu$_2$O [s^{-1} atm^{-1}]
$P_{O_2,ave}$	Logarithmic average of partial pressure of oxygen [atm]
$P_{O_2,eq}$	Equilibrium partial pressure of oxygen [atm]
$P_{O_2,in}$	Partial pressure of oxygen at the inlet of the reactor [atm]
$P_{O_2,out}$	Partial pressure of oxygen at the outlet of the reactor [atm]
$\dot{m}_{OC}$	Rate of solid flow between the two reactors [kg s^{-1} MW$_{th}^{-1}$]

BIBLIOGRAPHY

(1) Basu, P. *Combustion and Gasification in Fluidized Beds*; CRC Press, Taylor & Francis Group: Boca Raton, 2006.

(2) Stafford, N. Trillions for CCS to fight climate change. *RSC Publishing* 2009, http://www.rsc.org/chemistryworld/News/2009/October/21100901.asp (Accessed 11th September 2012).

(3) Friedlingstein, P.; Houghton, R. A.; Marland, G.; Hackler, J.; Boden, T. A.; Conway, T. J.; Canadell, J. G.; Raupach, M. R.; Ciais, P.; Le Quere, C. Update on CO_2 emissions. *Nature Geosci* 2010, 3 (12), 811-812.

(4) Pachauri, R. K.; Reisinger, A. *Fourth Assesment Report: Climate Change (Synthesis Report)*; Intergovernmental Panel on Climate Change: Geneva, 2007.

(5) Herzog, H. J., CO_2 capture and storage: Costs and market potential. In *Greenhouse Gas Control Technologies 7*, Rubin, E. S.; Keith, D. W.; Gilboy, C. F.; Wilson, M.; Morris, T.; Gale, J.; Thambimuthu, K.; Thambimuthu, K., Eds. Elsevier Science Ltd: Oxford, 2005; pp 21-28.

(6) Toftegaard, M. B.; Brix, J.; Jensen, P. A.; Glarborg, P.; Jensen, A. D. Oxy-fuel combustion of solid fuels. *Progr. Energy Combust. Sci.* 2010, 36 (5), 581-625.

(7) Metz, B.; Davidson, O.; de Coninck, H.; Loos, M.; Meyer, L. *Special Report: Carbon Dioxide Capture and Storage*; Intergovernmental Panel on Climate Change: Cambridge 2005.

(8) Lyngfelt, A.; Leckner, B.; Mattisson, T. A fluidized-bed combustion process with inherent CO_2 separation; application of chemical-looping combustion. *Chem. Eng. Sci.* 2001, 56 (10), 3101-3113.

(9) Ishida, M.; Jin, H. A Novel Chemical-Looping Combustor without NO_x Formation. *Ind. Eng. Chem. Res.* 1996, 35 (7), 2469-2472.

(10) Kronberger, B.; Johansson, E.; Löffler, G.; Mattisson, T.; Lyngfelt, A.; Hofbauer, H. A Two-Compartment Fluidized Bed Reactor for CO_2 Capture by Chemical-Looping Combustion. *Chem. Eng. Technol.* 2004, 27 (12), 1318-1326.

(11) Jerndal, E.; Mattisson, T.; Lyngfelt, A. Thermal Analysis of Chemical-Looping Combustion. *Chem. Eng. Res. Des.* 2006, 84 (9), 795-806.

(12) Lyngfelt, A. Oxygen Carriers for Chemical Looping Combustion - 4000 h of Operational Experience. *Oil Gas Sci. Technol.* 2011, 66 (2), 161-172

(13) Lyngfelt, A.; Mattisson, T. *Materials for chemical-looping combustion*; WILEY-VCH Verlag GmbH & Co. KGaA: Weinheim, 2011.

(14) Hossain, M. M.; de Lasa, H. I. Chemical-looping combustion (CLC) for inherent CO_2 separations-a review. *Chem. Eng. Sci.* 2008, 63 (18), 4433-4451.

(15) Adanez, J.; Abad, A.; Garcia-Labiano, F.; Gayan, P.; de Diego, L. F. Progress in Chemical-Looping Combustion and Reforming technologies. *Progr. Energy Combust. Sci.* 2012, 38 (2), 215-282.

(16) Mattisson, T.; Lyngfelt, A.; Leion, H. Chemical-looping with oxygen uncoupling for combustion of solid fuels. *Int. J. Greenhouse Gas Control* 2009, 3 (1), 11-19.

(17) Cho, P.; Mattisson, T.; Lyngfelt, A. Comparison of iron-, nickel-, copper- and manganese-based oxygen carriers for chemical-looping combustion. *Fuel* 2004, 83 (9), 1215-1225.

(18) Wang, X.; Jin, B.; Zhong, W.; Zhang, Y.; Song, M. Three-dimensional simulation of a coal gas fueled chemical looping combustion process. *Int. J. Greenhouse Gas Control* 2011, 5 (6), 1498-1506.

(19) Adánez-Rubio, I.; Gayán, P.; Abad, A.; de Diego, L. F.; García-Labiano, F.; Adánez, J.

Evaluation of a Spray-Dried $CuO/MgAl_2O_4$ Oxygen Carrier for the Chemical Looping with Oxygen Uncoupling Process. *Energy Fuels* 2012, 26 (5), 3069-3081.

(20) Gayán, P.; Adánez-Rubio, I.; Abad, A.; de Diego, L. F.; García-Labiano, F.; Adánez, J. Development of Cu-based oxygen carriers for Chemical-Looping with Oxygen Uncoupling (CLOU) process. *Fuel* 2012, 96, 226-238.

(21) de Diego, L. F.; Gayán, P.; García-Labiano, F.; Celaya, J.; Abad, A.; Adánez, J. Impregnated CuO/Al_2O_3 Oxygen Carriers for Chemical-Looping Combustion: Avoiding Fluidized Bed Agglomeration. *Energy Fuels* 2005, 19 (5), 1850-1856.

(22) Chuang, S. Y.; Dennis, J. S.; Hayhurst, A. N.; Scott, S. A. Development and performance of Cu-based oxygen carriers for chemical-looping combustion. *Combust. Flame* 2008, 154 (1-2), 109-121.

(23) Hoteit, A.; Chandel, M. K.; Delebarre, A. Nickel- and Copper-Based Oxygen Carriers for Chemical Looping Combustion. *Chem. Eng. Technol.* 2009, 32 (3), 443-449.

(24) Corbella, B. M.; De Diego, L.; García, F.; Adánez, J.; Palacios, J. M. The Performance in a Fixed Bed Reactor of Copper-Based Oxides on Titania as Oxygen Carriers for Chemical Looping Combustion of Methane. *Energy Fuels* 2005, 19 (2), 433-441.

(25) Corbella, B. M.; de Diego, L.; García-Labiano, F.; Adánez, J.; Palacios, J. M. Characterization and Performance in a Multicycle Test in a Fixed-Bed Reactor of Silica-Supported Copper Oxide as Oxygen Carrier for Chemical-Looping Combustion of Methane. *Energy Fuels* 2005, 20 (1), 148-154.

(26) Gayán, P.; Forero, C. R.; Abad, A.; de Diego, L. F.; García-Labiano, F.; Adánez, J. Effect of Support on the Behavior of Cu-Based Oxygen Carriers during Long-Term CLC Operation at Temperatures above 1073 K. *Energy Fuels* 2011, 25 (3), 1316–1326.

(27) Abad, A.; Adánez-Rubio, I.; Gayán, P.; García-Labiano, F.; de Diego, L. F.; Adánez, J. Demonstration of chemical-looping with oxygen uncoupling (CLOU) process in a 1.5 kW$_{th}$ continuously operating unit using a Cu-based oxygen-carrier. *Int. J. Greenhouse Gas Control* 2012, 6, 189-200.

(28) Forero, C. R.; Gayán, P.; García-Labiano, F.; de Diego, L. F.; Abad, A.; Adánez, J. High temperature behaviour of a $CuO/\gamma Al_2O_3$ oxygen carrier for chemical-looping combustion. *Int. J. Greenhouse Gas Control* 2011, 5 (4), 659-667.

(29) de Diego, L. F.; García-Labiano, F.; Gayán, P.; Celaya, J.; Palacios, J. M.; Adánez, J. Operation of a 10 kWth chemical-looping combustor during 200 h with a $CuO-Al_2O_3$ oxygen carrier. *Fuel* 2007, 86 (7-8), 1036-1045.

(30) Adánez, J.; Gayán, P.; Celaya, J.; de Diego, L. F.; García-Labiano, F.; Abad, A. Chemical Looping Combustion in a 10 kW$_{th}$ Prototype Using a CuO/Al_2O_3 Oxygen Carrier: Effect of Operating Conditions on Methane Combustion. *Ind. Eng. Chem. Res.* 2006, 45 (17), 6075-6080.

(31) Zafar, Q.; Mattisson, T.; Gevert, B. Redox Investigation of Some Oxides of Transition-State Metals Ni, Cu, Fe, and Mn Supported on SiO_2 and $MgAl_2O_4$. *Energy Fuels* 2005, 20 (1), 34-44.

(32) Wang, S.; Luo, M.; Wang, G.; Wang, L.; Lv, M. Analysis of Reactivity of a CuO-Based Oxygen Carrier for Chemical Looping Combustion of Coal. *Energy Fuels* 2012, 26 (6), 3275-3283.

(33) Adánez, J.; de Diego, L. F.; García-Labiano, F.; Gayán, P.; Abad, A.; Palacios, J. M. Selection of Oxygen Carriers for Chemical-Looping Combustion. *Energy Fuels* 2004, 18 (2), 371-377.

(34) de Diego, L. F.; GarcIa-Labiano, F.; Adánez, J.; Gayán, P.; Abad, A.; Corbella, B. M.; MarIa Palacios, J. Development of Cu-based oxygen carriers for chemical-looping combustion. *Fuel* 2004, 83 (13), 1749-1757.

(35) Mattisson, T.; Järdnäs, A.; Lyngfelt, A. Reactivity of Some Metal Oxides Supported on Alumina with Alternating Methane and OxygenApplication for Chemical-Looping Combustion. *Energy Fuels* 2003, 17 (3), 643-651.

(36) Adánez, J.; García-Labiano, F.; de Diego, L. F.; Gayán, P.; Celaya, J.; Abad, A. Nickel–Copper

Oxygen Carriers To Reach Zero CO and H_2 Emissions in Chemical-Looping Combustion. *Ind. Eng. Chem. Res.* 2006, 45 (8), 2617-2625.

(37) Dennis, J. S.; Müller, C. R.; Scott, S. A. In situ gasification and CO_2 separation using chemical looping with a Cu-based oxygen carrier: Performance with bituminous coals. *Fuel* 2010, 89 (9), 2353-2364.

(38) Wang, B.; Zhao, H.; Zheng, Y.; Liu, Z.; Yan, R.; Zheng, C. Chemical looping combustion of a Chinese anthracite with Fe_2O_3-based and CuO-based oxygen carriers. *Fuel Process. Technol.* 2012, 96 (0), 104-115.

(39) Mattisson, T.; Leion, H.; Lyngfelt, A. Chemical-looping with oxygen uncoupling using CuO/ZrO_2 with petroleum coke. *Fuel* 2009, 88 (4), 683-690.

(40) Smyth, F. H.; Roberts, H. S. THE SYSTEM CUPRIC OXIDE, CUPROUS OXIDE, OXYGEN. *J. Am. Chem. Soc.* 1920, 42 (12), 2582-2607.

(41) Wen, Y.-y.; Li, Z.-s.; Xu, L.; Cai, N.-s. Experimental Study of Natural Cu Ore Particles as Oxygen Carriers in Chemical Looping with Oxygen Uncoupling (CLOU). *Energy Fuels* 2012, 26, 3919-3927.

(42) Saha, C.; Bhattacharya, S. Comparison of CuO and NiO as oxygen carrier in chemical looping combustion of a Victorian brown coal. *Int. J. Hydrogen Energy* 2011, 36 (18), 12048-12057.

(43) Siriwardane, R.; Tian, H.; Richards, G.; Simonyi, T.; Poston, J. Chemical-Looping Combustion of Coal with Metal Oxide Oxygen Carriers. *Energy Fuels* 2009, 23 (8), 3885-3892.

(44) Eyring, E. M.; Konya, G.; Lighty, J. S.; Sahir, A. H.; Sarofim, A. F.; Whitty, K. Chemical Looping with Copper Oxide as Carrier and Coal as Fuel. *Oil Gas Sci. Technol.* 2011, 66 (2), 209-221.

(45) Chuang, S. Y.; Dennis, J. S.; Hayhurst, A. N.; Scott, S. A. Kinetics of the chemical looping oxidation of H_2 by a co-precipitated mixture of CuO and Al_2O_3. *Chem. Eng. Res. Des.* 2011, 89 (9), 1511-1523.

(46) Rasband, W. S. *ImageJ*, National Institutes of Health: Bethesda, 1997.

(47) Chuang, S. Y.; Dennis, J. S.; Hayhurst, A. N.; Scott, S. A. Kinetics of the Oxidation of a Co-precipitated Mixture of Cu and Al_2O_3 by O_2 for Chemical-Looping Combustion. *Energy Fuels* 2010, 24 (7), 3917-3927.

(48) Chadda, D.; Ford, J. D.; Fahim, M. A. Chemical Energy Storage by the Reaction Cycle CuO/Cu_2O *Int. J. Energy Res.* 1989, 13 (63), 63-73.

(49) Landolt-Börnstein, Thermodynamic Properties of Inorganic Material (SGTE). In Springer-Verlag, Berlin-Heidelberg: 1999; Vol. Part 1.

(50) Knacke, O.; Kubaschewski, O.; Hesselman, K. *Thermochemical properties of inorganic substances*; Springer-Verlag: Berlin, 1991.

(51) Jacob, K. T.; Alcock, C. B. Thermodynamics of $CuAlO_2$ and $CuAl_2O_4$ and Phase Equilibria in the System Cu_2O-CuO-Al_2O_3. *J. Am. Ceram. Soc.* 1975, 58 (5-6), 192-195.

(52) Gadalla, A. M. M.; White, J. Equilibrium Relationships in the System CuO-Cu_2O-Al_2O_3. *J. Brit. Ceram. Soc.* 1964, 63 (1), 39-62.

(53) Tsuchida, T.; Furuichi, R.; Sukegawa, T.; Furudate, M.; Ishii, T. Thermoanalytical study on the reaction of the CuO-Al_2O_3 (η, g, and a) systems. *Thermochim. Acta* 1984, 78 (1-3), 71-80.

(54) Susnitzky, D. W.; Carter, C. B. The formation of copper aluminate by solid-state reaction. *J. Mater. Res.* 1991, 6 (09), 1958-1963

(55) Bolt, P. H.; Habraken, F. H. P. M.; Geus, J. W. Formation of Nickel, Cobalt, Copper, and Iron Aluminates from α- and g-Alumina-Supported Oxides: A Comparative Study. *J. Solid State Chem.* 1998, 135 (1), 59-69.

(56) Tang, Y.; Chui, S. S.-Y.; Shih, K.; Zhang, L. Copper Stabilization via Spinel Formation during the Sintering of Simulated Copper-Laden Sludge with Aluminum-Rich Ceramic Precursors.

Environ. Sci. Technol. 2011, 45 (8), 3598–3604.

(57) Tsuboi, N.; Itoh, Y.; Ogata, J.; Kobayashi, S.; Shimizu, H.; Kato, K.; Kaneko, F. Composition and Structure Control of Cu–Al–O Films Prepared by Reactive Sputtering and Annealing. *Japanese Journal of Applied Physics* 2007, 46 (1), 351–355.

(58) Woelk, H.-J.; Hoffmann, B.; Mestl, G.; Schloegl, R. Experimental Archaeology: Investigation on the Copper–Aluminum–Silicon–Oxygen System. *J. Am. Ceram. Soc.* 2002, 85 (7), 1876-1878.

(59) Patrick, V.; Gavalas, G. R.; Flytzani-Stephanopoulos, M.; Jothimurugesan, K. High-temperature sulfidation-regeneration of copper(II) oxide-alumina sorbents. *Ind. Eng. Chem. Res.* 1989, 28 (7), 931-940.

(60) Patrick, V.; Gavalas, G. Structure and Reduction and Mixed Copper-Aluminum Oxide. *J. Am. Ceram. Soc.* 1990, 73 (2), 358-369.

(61) Zalazinskii, A. G.; Balakirev, V. F.; Chebotaev, N. M.; Chufarov, G. I. Thermodynamic Analysis of the Reduction, Dissociation, and Formation of Copper (I) Aluminate ($CuAlO_2$), Chromate(III) ($CuCrO_2$), and Ferrate(II) ($CuFeO_2$) from the Free Elements and Oxides. *Russ. J. Inorg. Chem.* 1969, 14 (3), 326-328.

(62) Kumekawa, Y.; Hirai, M.; Kobayashi, Y.; Endoh, S.; Oikawa, E.; Hashimoto, T. Evaluation of thermodynamic and kinetic stability of $CuAlO_2$ and $CuGaO_2$. *J. Therm. Anal. Calorim.* 2010, 99 (1), 57-63.

(63) Khawam, A.; Flanagan, D. R. Solid-State Kinetic Models: Basics and Mathematical Fundamentals. *The Journal of Physical Chemistry B* 2006, 110 (35), 17315-17328.

(64) Monazam, E. R.; Siriwardane, R.; Breault, R. W.; Tian, H.; Shadle, L. J.; Richards, G.; Carpenter, S. Kinetics of the Reduction of CuO/Bentonite by Methane (CH_4) during Chemical Looping Combustion. *Energy Fuels* 2012, 26 (5), 2779-2785.

(65) Abad, A.; Adánez, J.; García-Labiano, F.; de Diego, L. F.; Gayán, P.; Celaya, J. Mapping of the range of operational conditions for Cu-, Fe-, and Ni-based oxygen carriers in chemical-looping combustion. *Chem. Eng. Sci.* 2007, 62 (1-2), 533-549.

(66) Adánez-Rubio, I.; Abad, A.; Gayán, P.; de Diego, L. F.; García-Labiano, F.; Adánez, J. Identification of operational regions in the Chemical-Looping with Oxygen Uncoupling (CLOU) process with a Cu-based oxygen carrier. *Fuel* 2012, 102, 635-645.